

Tunable backaction of a dc SQUID on an integrated micromechanical resonator

M. Poot,^{1,*} S. Etaki,^{1,2} I. Mahboob,² K. Onomitsu,² H. Yamaguchi,² Ya. M. Blanter,¹ and H. S. J. van der Zant¹

¹*Kavli Institute of Nanoscience, Delft University of Technology,
Post Office Box 5046, 2600 GA Delft, Netherlands*

²*NTT Basic Research Laboratories, NTT Corporation, Atsugi-shi, Kanagawa 243-0198, Japan
(Dated: November 15, 2018)*

We have measured the backaction of a dc superconducting quantum interference device (SQUID) position detector on an integrated 1 MHz flexural resonator. The frequency and quality factor of the micromechanical resonator can be tuned with bias current and applied magnetic flux. The backaction is caused by the Lorentz force due to the change in circulating current when the resonator displaces. The experimental features are reproduced by numerical calculations using the resistively and capacitively shunted junction (RCSJ) model.

It has recently been demonstrated that a macroscopic mechanical resonator can be put in a quantum state [1] by coupling it to another quantum system. At the same time, linear detectors coupled to mechanical resonators are rapidly approaching the quantum limit on position detection. This limit implies that the resonator position cannot be measured with arbitrary accuracy, as the detector itself affects the resonator position [2]. This is an example of backaction. Backaction does not just impose limits, it can also work to one's advantage: Backaction can cool the resonator, squeeze its motion, and couple and synchronize multiple resonators. Different backaction mechanisms have been identified: When using optical interferometers [3–6] or electronic resonant circuits [7–9], backaction results from radiation pressure. In single-electron transistors (SET) [10], Cooper-pair boxes [11], carbon nanotube quantum dots [12, 13], or atomic and quantum point contacts [14, 15] backaction is due to the tunneling of electrons. Recently, we have used a dc SQUID as a sensitive detector of the position of an integrated mechanical resonator [16]. This embedded resonator-SQUID geometry enables the experimental realization of a growing number of theoretical proposals for which a good understanding of the backaction is required [17–23].

In this Letter, we present experiments that show that the dc SQUID detector exerts backaction on the resonator. By adjusting the bias conditions of the dc SQUID the frequency and damping of the mechanical resonator change. The backaction by the dc SQUID has a different origin than in the experiments mentioned above: It is due to the Lorentz force generated by the circulating current. Numerical calculations using the RCSJ model for the dc SQUID [24] reproduce the experimental features.

The device (Fig. 1a) consists of a dc SQUID with proximity-effect-based junctions [16]. A part of one arm is underetched, forming a 1 MHz flexural resonator with length $\ell = 50 \mu\text{m}$. In this Letter we present data on a device in an in-plane magnetic field of $B = 100 \text{ mT}$. Measurements have been performed at several magnetic fields and on an additional device; the observed back-

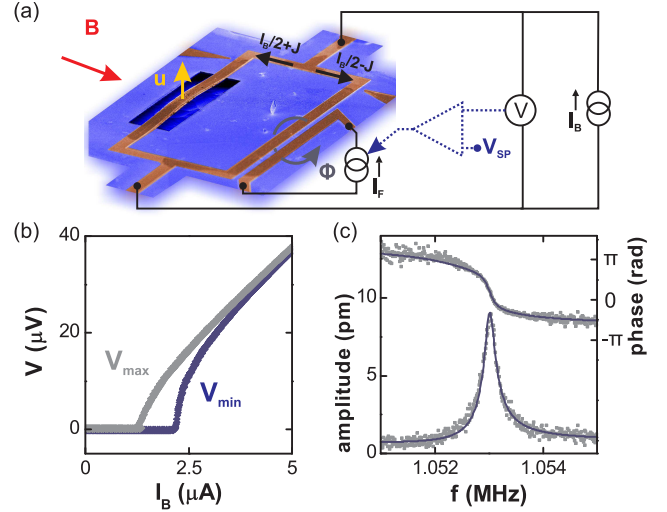


FIG. 1: (a) Schematic overview of the dc SQUID with the suspended beam and measurement setup. A magnetic field B transduces a beam displacement u into a change in magnetic flux. A bias current I_B is sent through the SQUID and its output voltage is measured. The flux Φ is fine-tuned with a stripline current I_F that is controlled by a feedback circuit (dashed) that keeps the output voltage V at V_{SP} . (b) The bias current dependence of the measured V_{\min} and V_{\max} . (c) The amplitude (bottom) and phase (top) response. The line is a fitted harmonic oscillator response [33].

action is similar [25]. First the dc SQUID is characterized. The output voltage of a dc SQUID depends on the magnetic flux through its loop Φ [24] and we measure the minimum and maximum voltage (V_{\min} and V_{\max}) by sweeping the flux over a few flux quanta $\Phi_0 = h/2e$ with a nearby stripline (Fig. 1a). This is repeated for different bias currents to obtain the current-voltage curves shown in Fig. 1b. The maximum critical current is $I_c^{\max} = 2.19 \mu\text{A}$ and the normal-state resistance of the junctions is $R = 15.6 \Omega$. After this characterization, the dc SQUID is operated at a given setpoint voltage V_{SP} using a feedback loop that adjusts the flux via the stripline current [16, 24]. The feedback loop is used to reduce

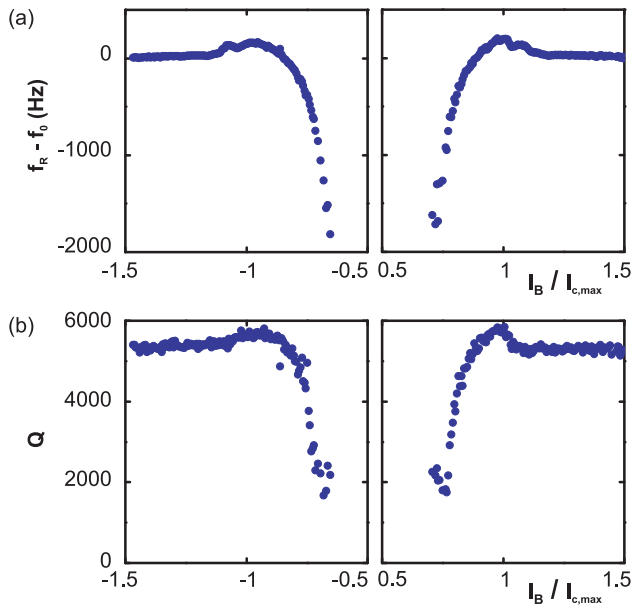


FIG. 2: Frequency shift (a) and quality factor (b) plotted versus the normalized bias current. The voltage setpoint was halfway between V_{min} and V_{max} in these measurements.

low-frequency flux noise and flux drift and has a bandwidth of ~ 2 kHz, i.e., it does not respond to the 1 MHz resonator signal.

The fundamental mode of the flexural resonator is excited using a piezo element underneath the sample and the displacement of the beam is detected as follows: The in-plane magnetic field transduces a displacement of the beam u into a flux change $\sim \ell B u$, which in turn changes the voltage over the dc SQUID. This voltage is amplified using a cryogenic high-electron mobility transistor followed by a room temperature amplifier and then recorded using a network analyzer. Figure 1c shows the amplitude and phase of the measured response, from which the resonance frequency f_R and quality factor Q are obtained.

To observe backaction of the dc SQUID detector on the resonator, the frequency response is measured for different bias conditions of the SQUID. Figure 2 shows that both f_R and Q depend on the bias current I_B . The resonance frequency saturates at $f_0 = 1.053010$ MHz for large positive and negative bias currents. However, when decreasing the I_B , f_R first goes up by a few hundred Hz around I_c^{max} and then it decreases rapidly with about -2000 Hz at the lowest stable setpoint voltage. This is more than $10\times$ the linewidth $f_R/Q = 194$ Hz of the resonance shown in Fig. 1c. Figure 2b shows that the quality factor of the resonator changes from $Q_0 = 5300$ to less than 2000. Similar to the resonance frequency, first an increase and then a stronger decrease in Q is observed when lowering the bias current. Figure 3 shows that the frequency and damping can also be changed by adjusting V_{SP} , i.e., the flux through the SQUID loop. The shifts

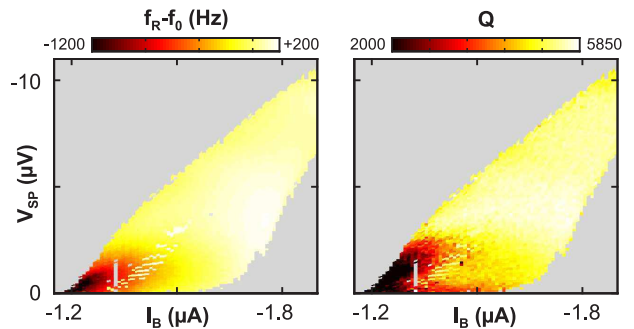


FIG. 3: Measured bias current and voltage setpoint dependence of the frequency shift (left) and damping (right). Points without a good lock are indicated in gray.

are largest for low setpoints and low bias currents (dark regions). The regions with a lower frequency coincide with the regions where the damping has increased. Bias points with positive frequency shifts and increases in Q are indicated in white. Finally, by varying the driving power we confirm that the observed effects are not due to nonlinearities in the SQUID or in the resonator [25].

Unlike for position detectors such as the SET where the backaction originates from the Coulomb force, the backward coupling between the SQUID and the beam is the Lorentz force F_L [18, 21]. This force is due to the current that flows through the beam in the presence of the magnetic field that couples the resonator and the SQUID. A displacement changes the flux, and this in turn changes the circulating current in the loop J [24], giving a different force on the beam. In addition, resonator motion yields a time-varying flux through the loop, which induces an electro-motive force and thereby also generates currents that change the Lorentz force [26].

The displacement of the fundamental out-of-plane flexural mode u is given by [27]:

$$m\ddot{u} + m\omega_0\dot{u}/Q_0 + m\omega_0^2u = F_d(t) + F_L(t). \quad (1)$$

The resonator has a mass m , (intrinsic) frequency $f_0 = \omega_0/2\pi$ and quality factor Q_0 . F_d is the driving force and $F_L = aBl(I_B/2 + J)$ is the Lorentz force. Here, $a = (u\ell)^{-1} \int_0^\ell u(x) dx \approx 0.9$ for the fundamental mode, so that also $\partial\Phi/\partial u = aBl$ [16, 27]. For small amplitudes and low resonator frequencies (much smaller than the characteristic SQUID frequency $\omega_c = \pi RI_c^{max}/\Phi_0$), the average circulating current can be expanded in the displacement and velocity \dot{u} [25]:

$$J(u, \dot{u}) = J_0 + \frac{\partial J}{\partial \Phi} aBl u + \frac{\partial J}{\partial \dot{\Phi}} aBl \dot{u}. \quad (2)$$

Inserting Eq. (2) into Eq. (1) shows that the $\partial J/\partial \Phi$ term affects the spring constant $m\omega_R^2$ and thus f_R , whereas the $\partial J/\partial \dot{\Phi}$ term renormalizes the damping. The shifted

resonance frequency and quality factor are:

$$f_R = f_0 (1 - \Delta_f J_\phi)^{1/2}, \text{ with } \Delta_f = \frac{a^2 B^2 \ell^2 I_c^{\max}}{m\omega_0^2 2\Phi_0}, \quad (3)$$

$$Q = Q_0 \frac{f_R}{f_0} \frac{1}{1 - \Delta_Q J_\phi}, \text{ with } \Delta_Q = \frac{a^2 B^2 \ell^2 Q_0}{m\omega_0 R 2\pi}. \quad (4)$$

Here, $J_\phi = \partial J / \partial \Phi \times 2\Phi_0 / I_c^{\max}$ and $J_\dot{\phi} = \partial J / \partial \dot{\Phi} \times 2\omega_c \Phi_0 / I_c^{\max}$ are the scaled flux-to-current transfer functions [28]. The former indicates how much the circulating current changes when the flux through the ring is altered, whereas the latter quantifies the effect of a time-dependent flux on the circulating current. These functions were first studied in the analysis of the dynamic input impedance of tuned SQUID amplifiers [28, 29] and are intrinsic properties of the SQUID.

Before looking in more detail at the transfer functions, we first focus on the coupling. The dimensionless parameters Δ_f [20] and Δ_Q characterize the backaction strength. They contain the term aBl squared as both the flux change and the Lorentz force are proportional to the magnetic field. This implies that the backaction remains the same when the direction of the magnetic field is reversed and this is what we observe experimentally. Δ_f is proportional to I_c^{\max} , whereas the damping induced by the SQUID depends on R . By a careful design of the resonator and SQUID, the backaction strengths can be tuned over a wide range. Eqs. (3) and (4) show that the largest backaction occurs for large flux changes aBl , low spring constants $m\omega_0^2$, and large circulating currents, i.e., large I_0 and low R . For the device studied in this Letter, we estimate $\Delta_f = 4.1 \times 10^{-4}$ and $\Delta_Q = 2.8 \times 10^{-4}$. Finally, note that the two coupling parameters are related by $\Delta_Q = \Delta_f \times Q_0 \omega_0 / \omega_c$.

So far, the analysis did not assume anything about the number of junctions, nor about their microscopic details. To obtain the transfer functions J_ϕ and $J_\dot{\phi}$, we model the junctions in the dc SQUID using the RCSJ model [24]. The transfer functions can be calculated analytically in certain limits [30]. However, to obtain their full bias-condition dependence, J_ϕ and $J_\dot{\phi}$ must be calculated numerically. This is done by simulating the dynamics of the SQUID in the presence of a time-varying flux [25]. Figure 4a shows the bias-dependence of J_ϕ . In the region where $V = 0$, the circulating current redistributes the bias current between the two junctions such that no voltage develops. Here the circulating current is of the order of $I_c^{\max}/2$, which gives $J_\phi \sim -1$ (blue). In the dissipative region ($V \neq 0$), the circulating current is suppressed. Therefore, the circulating current changes rapidly close to the edge of the dissipative region. The orange color in Fig. 4a indicates that J_ϕ is large and positive near the critical current. The largest downward frequency shift is expected near a half-integer number of flux quanta, whereas J_ϕ vanishes for integer flux. With the value of the coupling parameter Δ_f and the resonance

frequency f_0 the frequency shift is calculated as shown in Fig. 4c. The maximum value $J_\phi = 53$ gives a frequency shift of -12 kHz in the lower-left corner, which has to be compared with the experimental value of ~ -2 kHz. Increasing the bias current above the critical current results in a smaller J_ϕ (light yellow and light blue) that depends linearly on the inductive screening parameter β_L [24] for the experimental conditions. In this region the simulations predict both positive (blue) and negative (yellow) value for J_ϕ . Positive and negative shifts are also observed in the experiment (Figs. 2 and 3). The largest negative value found in the simulations of that region is $J_\phi = -0.65$, which results in an increase in f_R of ~ 140 Hz, which is in agreement with the observed value of ~ 200 Hz (Fig. 2a). For even larger bias currents, the frequency shift vanishes $f_R \approx f_0$. This corresponds to the flat regions in Fig. 2a.

The change in damping is determined by $J_\dot{\phi}$ as indicated by Eq. (4). Its dependence on the bias conditions is shown in Fig. 4b. Well inside the experimentally inaccessible non-dissipative region $J_\dot{\phi} \sim +1$ and the backaction results in a small increase in Q . In the opposite limit of large bias currents $J_\dot{\phi} = -\pi$ (light blue). This value combined with the small value of Δ_Q implies that the quality factor in the flat region in Fig. 2b is close to the intrinsic Q-factor, Q_0 . In this region the small additional damping is due to the current induced by the time-varying flux $\dot{\Phi}/2R$, which is dissipated in the junction resistances [30]. This contribution is well-known from magnetomotive readout of mechanical resonators [26]. When lowering the bias current, $J_\dot{\phi}$ changes sign and rises to about $+500$. This reduces the damping and might even lead to instability ($Q < 0$) if Δ_Q is large enough. This decrease of damping corresponds to the bumps in Fig. 2b. The largest observed quality factor $Q = 5800$ corresponds to $J_\dot{\phi} = +400$, which is in reasonable agreement with the simulations. Close to the critical current, $J_\dot{\phi}$ goes to large *negative* values leading to an enhanced dissipation. Figure 4d shows that the calculated Q-factor is indeed lowest near the critical current. In summary, our model shows that although the coupling strength is small, the dynamics of the dc SQUID greatly enhances the backaction.

Various interesting effects can be observed when the backaction is strong. If the resonator and SQUID are strongly coupled, the resonator temperature is set by the effective bath temperature [10, 14] of the SQUID. The increased damping cools the resonator, but the shot noise in the bias current leads to an increase in the force noise on the resonator, heating it. The question whether the resonator temperature is above or below the environmental temperature should be addressed in future research. Furthermore, the dependence of f_R and Q on the bias conditions allows parametric excitation of the mechanical resonator by either modulating the flux or the bias current. This enables squeezing of the thermomechanical

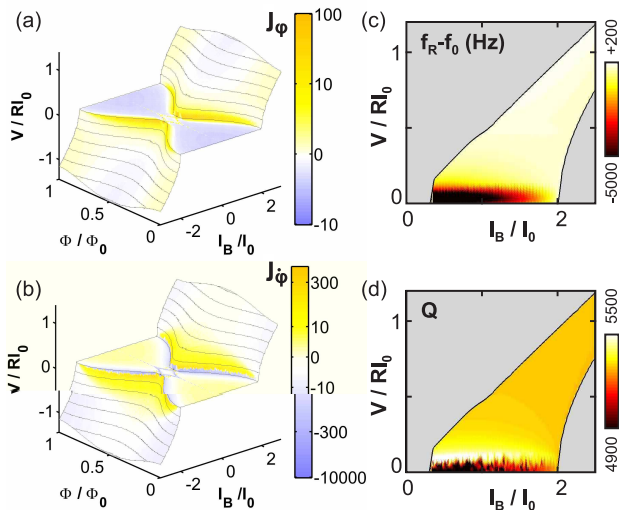


FIG. 4: Surface plots with iso-voltage lines at different bias conditions of a dc SQUID. The (logarithmic) color-scale represents the calculated flux-to-current transfer functions J_ϕ (a) and J_ϕ (b). With the values for Δ_f and Δ_Q , the frequency shift (c) and quality factor change (d) are calculated. The simulation is done for the experimental conditions where the inductive screening parameter $\beta_L = 0.21$ and the Stewart-McCumber parameter $\beta_C = 0.23$ [24, 25].

cal noise of the resonator [20, 31]. Finally, if the SQUID contains multiple, nearly identical mechanical resonators, these are coupled to each other by the backaction. This, in turn, can synchronize their motion and might lead to frequency entrainment if higher order terms in Eq. (2) become significant [32]. These examples are only a few intriguing possibilities of the rich physics connected to the backaction that we have described in this Letter.

We thank T. Akazaki, H. Okamoto and K. Yamazaki for help with fabrication and R. Schouten for the measurement electronics. This work was supported in part by JSPS KAKENHI (20246064 and 18201018), FOM, NWO (VICI grant), and a EU FP7 STREP project (QNEMS).

* Electronic address: m.poot@tudelft.nl

- [1] A. D. O'Connell et al., Nature **464**, 697 (2010).
- [2] C. M. Caves et al., Rev. Mod. Phys. **52**, 341 (1980).
- [3] S. Gigan et al., Nature **444**, 67 (2006).
- [4] O. Arcizet et al., Nature **444**, 71 (2006).
- [5] J. D. Thompson et al., Nature **452**, 72 (2008).
- [6] G. Anetsberger et al., Nat Phys **5**, 909 (2009).
- [7] J. D. Teufel et al., Phys. Rev. Lett. **101**, 197203 (pages 4) (2008).
- [8] K. R. Brown et al., Phys. Rev. Lett. **99**, 137205 (pages 4) (2007).
- [9] T. Rocheleau et al., Nature **463**, 72 (2010).
- [10] A. Naik et al., Nature **443**, 193 (2006).
- [11] M. D. LaHaye et al., Nature **459**, 960 (2009).

- [12] G. A. Steele et al., Science **325**, 1103 (2009).
- [13] B. Lassagne et al., Science **325**, 1107 (2009).
- [14] N. E. Flowers-Jacobs, D. R. Schmidt, and K. W. Lehnert, Phys. Rev. Lett. **98**, 096804 (pages 4) (2007).
- [15] J. Stettenheim et al., Nature **466**, 86 (2010).
- [16] S. Etaki et al., Nat Phys **4**, 785 (2008).
- [17] X. Zhou and A. Mizel, Phys. Rev. Lett. **97**, 267201 (pages 4) (2006).
- [18] M. P. Blencowe and E. Buks, Phys. Rev. B **76**, 014511 (pages 16) (2007).
- [19] F. Xue et al., Phys. Rev. B **76**, 064305 (pages 9) (2007).
- [20] W. Y. Huo and G. L. Long, Appl. Phys. Lett. **92**, 133102 (pages 3) (2008).
- [21] P. D. Nation, M. P. Blencowe, and E. Buks, Phys. Rev. B **78**, 104516 (pages 17) (2008).
- [22] E. Buks and M. P. Blencowe, Phys. Rev. B **74**, 174504 (pages 8) (2006).
- [23] F. Xue et al., New J. Phys. **9**, 35 (2007).
- [24] J. Clarke and A. Braginski, *The SQUID Handbook volume 1* (Wiley-VCH Verlag, GmbH and Co. KGaA, Weinheim, 2004).
- [25] See EPAPS Document No. [number will be inserted by publisher] for supplementary information. For more information on EPAPS, see <http://www.aip.org/pubser/s/epaps.html>.
- [26] A. N. Cleland and M. L. Roukes, Sens. Act. A **72**, 256 (1999).
- [27] A. N. Cleland and M. L. Roukes, J. Appl. Phys. **92**, 2758 (2002).
- [28] C. Hilbert and J. Clarke, J. Low Temp. Phys. **61**, 237 (1985).
- [29] P. Falferi et al., Applied Physics Letters **71**, 956 (1997).
- [30] Ya. M. Blanter, in preparation.
- [31] D. Rugar and P. Grütter, Phys. Rev. Lett. **67**, 699 (1991).
- [32] S.-B. Shim, M. Imboden, and P. Mohanty, Science **316**, 95 (2007).
- [33] Our fits take the small crosstalk between the driving signal and output voltage that is present in the experiment, into account. This effect makes the lineshape slightly asymmetric.
- [34] H. Yamaguchi, S. Miyashita, and Y. Hirayama, Appl. Surf. Sci. **237**, 645 (2004).
- [35] A. K. Hüttel et al., Nano Lett. **9**, 2547 (2009).
- [36] M. D. LaHaye et al., Science **304**, 74 (2004).
- [37] G. Zolfagharkhani et al., Phys. Rev. B **72**, 224101 (pages 5) (2005).

Temperature and power dependence

Figures 5a and b show the temperature dependence of the resonance frequency and quality factor. These values are measured at large bias currents where the backaction is negligible. The frequency change due to temperature is small compared to the observed backaction (see main text). The intrinsic quality factor decreases significantly with increasing temperature. This rules out that the observed frequency shift and Q-factor change are caused by heating of the resonator due to Joule heating in the junctions: We observe an *increase* in quality factor with increasing bias current and voltage setpoint (i.e. dissi-

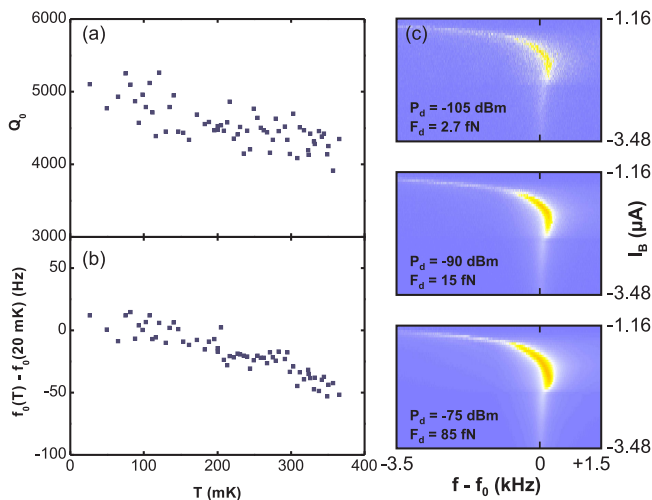


FIG. 5: Temperature dependence of the intrinsic quality factor Q_0 (a) and resonator frequency f_0 (b). (c) Colorscale plot of the oscillator response at $B = 100$ mT at different driving powers P_d . This measurement is done with a voltage setpoint halfway between V_{\min} and V_{\max} .

pation), but a *decrease* in quality factor with increasing temperature. An increased damping at higher temperatures is seen more often in micro- or nanomechanical resonators [34–37].

The observed frequency shift and change in damping do not depend on the driving power. As shown in Figure 5c, the measured resonator response stays the same in all panels. Although the driving power is changed by three orders of magnitude, the only effect is that the signal-to-noise ratio becomes better when increasing the power.

For the highest driving power ($P_d = -75$ dBm) and highest Q-factor ($Q \sim 5800$) the amplitude of the resonator motion is $u_{\max} = 20$ pm, as determined using the calibrated displacement responsivity [16]. The flux through the dc SQUID is then modulated with an amplitude $aBlu_{\max} = 0.02 \Phi_0$. So even for the largest resonator motion, the change in flux is much smaller than a flux quantum. Exactly on resonance, the piezo motion is Q times smaller than u_{\max} , about 3 fm. The driving force F_d is then given by the resonator mass m times the acceleration of the piezo element, $F_d = m\omega^2 u_p \approx m\omega_0^2 u_p$. The measurements shown in the main text are done with a driving power of -80 dBm ($F_d = 48$ fN).

Device B

All effects that we have observed in the device that we discuss in the main text have also been measured in a second device. The resonator in this dc SQUID operates around 2 MHz. The maximum critical current of device B is $I_c^{\max} = 2I_0 = 2.4 \mu\text{A}$ at $B = 115$ mT and $I_c^{\max} = 1.0 \mu\text{A}$ at $B = 130$ mT.

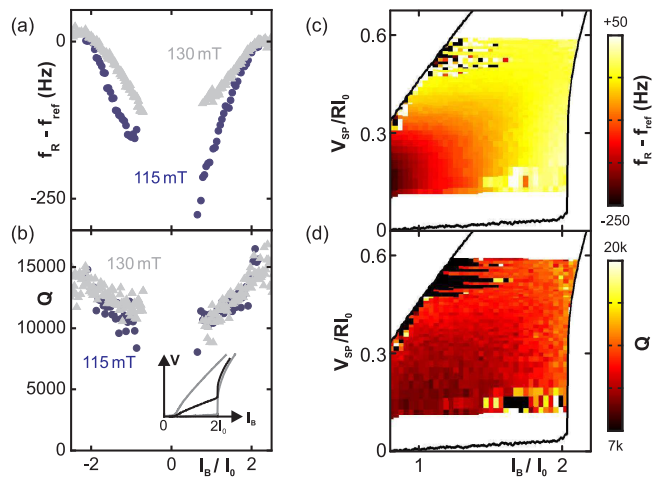


FIG. 6: Backaction measurements of device B. (a) Frequency shift and (b) quality factor plotted versus the normalized bias current at $B = 115$ mT (circles) and $B = 130$ mT (triangles). The inset depicts the voltage setpoint for these measurements with respect to V_{\min} and V_{\max} . Bias current and setpoint dependence of the frequency shift (c) and damping (d) at $B = 115$ mT. The solid lines indicate the measured V_{\min} and V_{\max} .

In the measurements on device B, the feedback loop could not maintain the SQUID voltage for low voltage setpoints. Also, a less sensitive, room temperature amplifier was used for the resonator signal. Its lower gain resulted in an increased scatter in the data and the inability to explore the region with the highest backaction, i.e., at low bias current and low voltage setpoints. The measurements in Fig. 6 show qualitatively the same backaction as the data presented in the main text.

The RCSJ model for the dc SQUID

To calculate the backaction, the dc SQUID is modelled using the resistively- and capacitively-shunted junction (RCSJ) model. This widely-used model is discussed in detail in Ref. [24]. The introduction to this model presented here is largely based on this review. A current I_B is sent through the SQUID and the circulating current J redistributes the current over the two junctions, which we assume to be identical. In the RCSJ model, the two junctions (labelled with $i = 1, 2$) are modelled as a resistor (R), capacitor (C) and an “ideal” Josephson junction with critical current I_0 in parallel. The voltage over each junction is related to the time derivative of the phase difference δ_i of the superconducting wave function: $V_i = \Phi_0 \dot{\delta}_i / 2\pi$, where $\Phi_0 = h/2e = 2.05 \times 10^{-15}$ Tm² is the flux quantum. Current conservation yields two second-order differential equations, governing the time-

dependence of the phase differences $\delta_{1,2}$ of the junctions:

$$\frac{\Phi_0}{2\pi} C \ddot{\delta}_1 + \frac{\Phi_0}{2\pi} \frac{1}{R} \dot{\delta}_1 + I_0 \sin \delta_1 = \frac{1}{2} I_B + J, \quad (5)$$

$$\frac{\Phi_0}{2\pi} C \ddot{\delta}_2 + \frac{\Phi_0}{2\pi} \frac{1}{R} \dot{\delta}_2 + I_0 \sin \delta_2 = \frac{1}{2} I_B - J. \quad (6)$$

These equations are coupled to each other by the amount of flux piercing the loop:

$$\delta_2 - \delta_1 = 2\pi \cdot \Phi_{\text{tot}} / \Phi_0. \quad (7)$$

The total flux Φ_{tot} has two contributions: the externally applied flux Φ (which also includes the flux due to the resonator displacement) and the flux due to the circulating current flowing through the inductance of the loop L , i.e., $\Phi_{\text{tot}} = \Phi + LJ$.

The equations are scaled to simplify their numerical integration. This yields:

$$\beta_C \ddot{\delta}_1 + \dot{\delta}_1 + \sin \delta_1 = \nu_B / 2 + j \quad (8)$$

$$\beta_C \ddot{\delta}_2 + \dot{\delta}_2 + \sin \delta_2 = \nu_B / 2 - j \quad (9)$$

$$2\pi(\phi + \beta_L j / 2) = \delta_2 - \delta_1. \quad (10)$$

The bias current and circulating current are normalized using the critical current: $\nu_B = I_B / I_0$ and $j = J / I_0$. Furthermore, time is scaled using the characteristic frequency $\omega_c = 2\pi R I_0 / \Phi_0$, fluxes using the flux quantum, i.e., $\phi = \Phi / \Phi_0$, and voltages using the characteristic voltage $R I_0$ so that $v = V / R I_0 = (\dot{\delta}_1 + \dot{\delta}_2) / 2$. The parameter $\beta_L = 2 I_0 L / \Phi_0$ and $\beta_C = 2\pi I_0 R^2 C / \Phi_0$ are the inductive screening parameter and the Stewart-McCumber number respectively. The inductive screening parameter indicates how much a change in flux is screened by the circulating current J flowing through the self-inductance of the loop L , whereas β_C indicates the importance of inertial terms due to the junction capacitance C .

The three equations are integrated numerically for different bias conditions, i.e., different values for the bias current I_B and for the flux Φ through the SQUID. Figure 7a shows typical examples of calculated time-traces of the circulating current j and voltage v . Both are rapidly oscillating at a frequency of $0.69 \omega_c$, which is the Josephson frequency that equals the average value of the voltage \bar{v} [24]. The maximum current that the dc SQUID can carry without generating a voltage equals the sum of the critical currents of the two junctions: $I_c^{\text{max}} = 2 I_0$.

The critical current ($I_0 = 1.1 \mu\text{A}$) and the normal-state resistance ($R = 15.6 \Omega$) of the junctions are estimated from the IV-characteristics (Fig. 1b of the main text). Using finite-element simulations we estimate $L = 175 \text{ pH}$ for our device. Finally, the capacitance $C = 0.6 \text{ pF}$ is obtained from the position of the LC resonance in the dc SQUID [24].

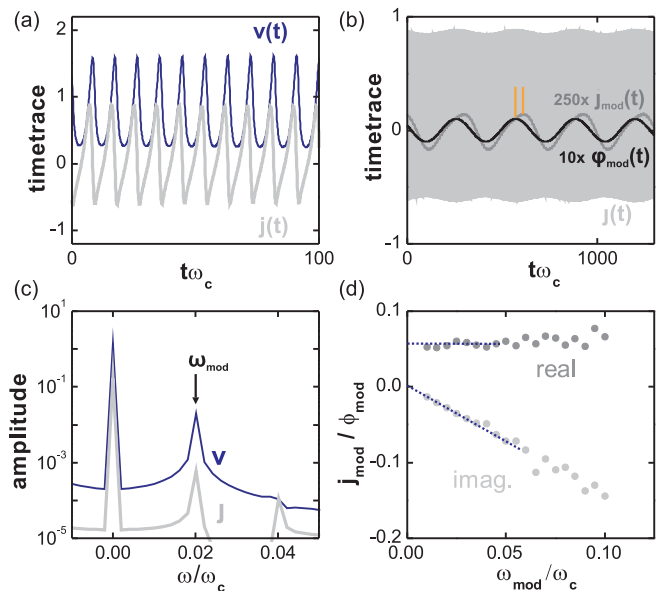


FIG. 7: (a) Calculated timetrace of the circulating current $j(t)$ and voltage $v(t)$ in the absence of noise. (b) Circulating current for a small ($\phi_{\text{mod}} = 0.01$) modulation of the flux with $\omega_{\text{mod}} = 0.02$. The time-averaged value of the circulating current $\bar{j}(t)$ has a phase shift with respect to the modulation $\phi(t)$ as indicated by the orange lines. (c) Absolute value of the Fourier transform of the timetraces of the SQUID voltage and circulating current shown in (b). (d) The modulation frequency dependence of the real (dark gray) and imaginary (light gray) parts of the transfer function. The lines are a guide to the eye. These simulations were done for the dc SQUID parameters from the main text ($\beta_L = 0.21$ and $\beta_C = 0.23$) at $\nu_B = 2$ and $\phi = 0.25$.

Calculation of the transfer functions

When the resonator moves, the flux through the dc SQUID loop is altered, which in turn changes the average circulating current J . In principle, $J(t)$ could depend on all the past displacements, $u(t')$ for $t' < t$. However, the dc SQUID reacts at a frequency ($\sim \omega_c / 2\pi \sim 8 \text{ GHz}$) that is much faster than that of the resonator (1 MHz), so the circulating current $J(t)$ is expected to depend on the *instantaneous* displacement $u(t)$. For small amplitudes ($u \ll \Phi_0 / aBl$) the response is linear and gives a contribution $J_1(t) = c_1 u(t)$. Another contribution comes from the velocity of the resonator, \dot{u} , which causes a time-varying flux. This generates an electromotive force in the SQUID loop (Faraday's induction law), which also changes the circulating current by $J_2(t) = c_2 \dot{u}(t)$. Combining these two effects gives $J(t) = J(u, \dot{u}) = c_1 u(t) + c_2 \dot{u}(t)$. The values of the parameters c_1 and c_2 depend on the dynamics of the dc SQUID and are $c_1 = \partial J / \partial u$ and $c_2 = \partial J / \partial \dot{u}$. As discussed in the main text, these quantities are related to the intrinsic flux-to-current transfer functions, $j_\phi = \Phi_0 / (aBl I_0) \times \partial J / \partial u$ and $j_{\dot{\phi}} = \omega_c \Phi_0 / (aBl I_0) \times \partial J / \partial \dot{u}$.

In principle j_ϕ can be obtained by calculating the average circulating current at different fluxes and then numerically differentiating this to obtain $j_\phi = \partial j / \partial \phi$. However, for the velocity-dependent transfer function this is not possible. Our method for calculating these transfer functions j_ϕ and $j_\dot{\phi}$ works as follows: We calculate the steady-state response of the circulating current with a small modulation added to the applied flux, $\phi \rightarrow \phi + \phi_{\text{mod}} \cos(\omega_{\text{mod}} t)$. Figure 7b shows that this modulates the circulating current $j(t)$. Figure 7c shows the Fourier transform of the circulating current and the

voltage. In the spectrum of both j and v a peak appears at the modulation frequency. The real part of the peak corresponds to the derivative $j_\phi = \text{Re}[j_{\text{mod}}/\phi_{\text{mod}}]$, while $\text{Im}[j_{\text{mod}}/\phi_{\text{mod}}] = -\omega_{\text{mod}} j_\dot{\phi}$ and similar for v_{mod} . The frequency dependence in Fig 7d, shows a constant $\text{Re}[j_{\text{mod}}]$ and a linearly increasing $\text{Im}[j_{\text{mod}}]$ as indicated by the dotted lines. The transfer functions do not depend on the modulation frequency, provided that it is sufficiently low. This confirms that the circulating current only depends on the instantaneous displacement and velocity as was postulated at the beginning of this Section.